Obstacle Avoidance Control for Two-Wheeled Drones Considering Sideslip Based on Control Barrier Functions

Keigo Mori[a], Satoshi Nakano[a], and Manabu Yamada[a]

[a]Graduate School of Engineering, Nagoya Institute of Technology; Gokiso-cho, Showa-ku, Nagoya, Aichi 466-8555, JAPAN

ARTICLE HISTORY
Compiled February 20, 2024

ABSTRACT

In this paper, we propose an obstacle avoidance control for two-wheeled drones considering sideslip based on control barrier functions. First, we derive the Lagrange equation of them on a wall. Next, we propose a trajectory tracking control law for them and prove that the equilibrium point of the system is almost global asymptotically stable. Then, we propose an obstacle avoidance control law for them considering sideslip on a wall. Finally, We confirm the effectiveness of the proposed control law for them by numerical simulations.

KEYWORDS
Drone; HyTAQs; Nonholonomic System; Trajectory Tracking; Cascade System; Stability; ECBF-QP; Obstacle Avoidance; Sideslip

1. Introduction

Exterior wall tiles used in many buildings can be peeled off and falled because of aging. In fact, it is mandatory to inspect them every 10 years. Normally, the inspection is carried out by engineers, but the inspection depends on the experience of the engineers and involves work at high places. Especially, among the labor accidents, the number of fatal accidents in construction industries is the highest, and the number of falling is the highest in construction industries. To solve such problems, it is expected that drones will conduct hammering tests and infrared inspections without depending on experience and with less risk. By manually controlling wheeled drones, engineers can inspect without taking risks. However, manual control depends on the experience of engineers.

Therefore, in this paper, we propose an autonomous control of two-wheeled drones. Research on autonomous control of drones without wheels [1–3] and research on autonomous control of HyTAQs (Hybrid Terrestrial and Aerial Quadrotors) [4–6] have been conducted. A two-wheeled drone has a system with a nonholonomic constraint. It is known that there is no continuous static state feedback controller that makes the origin of the system of a unicycle mobile robot almost global asymptotically stable [7]. Furthermore, the attitude of the two-wheeled drone is a nonlinear configuration

CONTACT Keigo Mori. Email: k.mori.452@stn.nitech.ac.jp

space with a unit circle, so there is no continuous static state feedback that makes the system global asymptotically stable [8]. Controllers for the two-wheeled drone with nonholonomic constraint has been proposed [9]. The two-wheeled drone has an additional degree of freedom because it is necessary to consider the rotation of pitch direction in addition to the rotation of a roll direction on a wall. Therefore, in this paper, we extend the attitude control, and propose the control law that includes dynamics not considered in [9]. Furthermore, since a drone has a cascade structure, it is necessary to consider the interconnection term [10] to discuss stability. We prove that the origin of the system of the two-wheeled drone with the control law in this paper is almost globally asymptotically stable [11].

In wall inspections, there is a risk that the drone will be damaged if it collides with windows, pipes, etc. when running on the wall, so the two-wheeled drone needs to avoid obstacles on a wall. Control barrier functions (CBF) has been studied in recent years to ensure the safety of systems [12–15]. For example, it has been applied to ACC (Adaptive Cruise Control) of automobiles [16,17] and obstacle avoidance for nonholonomic systems[18,19]. There are also studies on control laws using CBFs for drones to avoid obstacles [20,21]. In this paper, we use ECBF to avoid obstacles. In obstacle avoidance of the two-wheeled drone on a wall, the roll is likely to become large and it is easy to slip. On the other hand, by tilting the pitch and pressing the two-wheeled drone against a wall, it is less likely to slip. Therefore, we propose a control law to avoid slipping by modifying the torque of the pitch using control barrier function. Furthermore, we conduct numerical simulations using the proposed control law to verify the effectiveness.

2. Preliminaries

In this section, we derive the two-wheeled drone model and ECBF.

2.1. Two-wheeled drone model

Consider a two-wheeled drone moving on a wall illustrated in Fig. 1. We choose an inertial frame $e_i \in \mathbb{R}^3$, $i \in \{1,2,3\}$ and a body-fixed frame $\{b_x, b_y, b_z\}$. The origin of the body-fixed frame is the center of mass of the drone. The mass of the drone is $m \in \mathbb{R}$, acceleration of gravity is $g \in \mathbb{R}$, position in the world frame is $p = [x\ y\ z]^T \in \mathbb{R}^3$, body velocity is $v^b = [v_1^b\ v_2^b\ v_3^b]^T \in \mathbb{R}^3$, thrust is $f \in \mathbb{R}$, inertia tensor is $J \in \mathbb{R}^{3\times3}$, ZXY Euler angles is $\eta = [\alpha\ \beta\ \gamma]^T \in \mathbb{R}^3$, rotation matrix is $R \in SO(3)$, body angular velocity is $\omega^b = [\omega_1^b\ \omega_2^b\ \omega_3^b]^T \in \mathbb{R}^3$, body torque is $\tau^b \in \mathbb{R}^3$, and λ_j, $j \in \{1,2,3\}$ is Lagrangian multipliers. The two-wheeled drone running on the wall as shown in Fig. 1 has the following constraints,

(1) Not to slip on the wall.
(2) Constant distance from the wall.
(3) Not to rotate around the wall.

These constraints can be written as the following equation,

$$\begin{cases} f_1 &= v_2^b = r_{12}\dot{x} + r_{22}\dot{y} + r_{32}\dot{z} = 0 \\ f_2 &= x + \frac{D}{2} - L = 0 \\ f_3 &= e_1^T b_y = r_{12} = e_1^T(\eta - \eta_0) \end{cases} \tag{1}$$

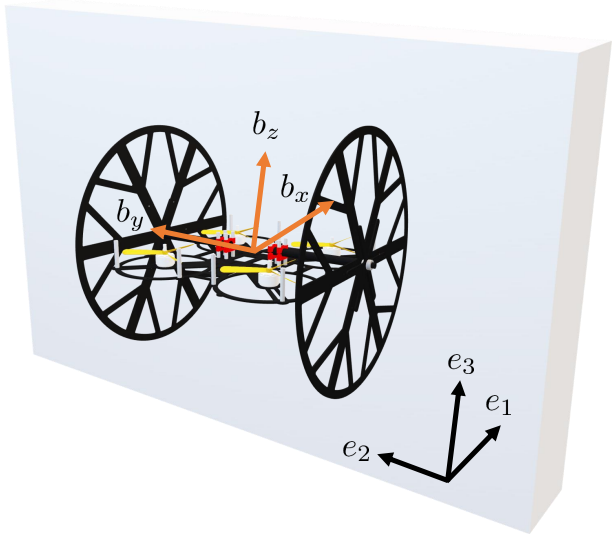

Figure 1. Two-wheeled drone moving on a wall.

where $D \in \mathbb{R}$ is the dismeter of the wheel, $L \in \mathbb{R}$ is the distance from the origin to the wall. From the third equation of (1), the first equation of (1) can be rewritten as follows,

$$f_1 = r_{22}\dot{y} + r_{32}\dot{z} = A\dot{p} = 0$$

where $A = [0\ r_{22}\ r_{32}]$.

The kinematics of the translational motion is given by

$$\dot{p} = Rv^b = \begin{bmatrix} 0 \\ -\frac{v_3^b \sin\beta}{\cos\gamma} \\ \frac{v_3^b \cos\beta}{\cos\gamma} \end{bmatrix} = \frac{1}{\cos\gamma} R_2(\beta)(v_3^b e_3) \tag{2}$$

where

$$\begin{aligned} R &= \begin{bmatrix} r_{11} & r_{12} & r_{13} \\ r_{21} & r_{22} & r_{23} \\ r_{31} & r_{32} & r_{33} \end{bmatrix} \\ &= \begin{bmatrix} \cos\gamma & 0 & \sin\gamma \\ \sin\beta\sin\gamma & \cos\beta & -\sin\beta\cos\gamma \\ -\cos\beta\sin\gamma & \sin\beta & \cos\beta\cos\gamma \end{bmatrix} \end{aligned}$$

$$R_2(\beta) = \begin{bmatrix} 1 & 0 & 0 \\ 0 & \cos\beta & -\sin\beta \\ 0 & \sin\beta & \cos\beta \end{bmatrix}.$$

The kinematics of the rotational motion in the ZXY Euler angles representation is

given by

$$\dot{\eta} = \Phi(\eta)\omega^b \tag{3}$$

where

$$\Phi(\eta) = \begin{bmatrix} \frac{\sin\gamma}{\cos\beta} & 0 & \frac{\cos\gamma}{\cos\beta} \\ \cos\gamma & 0 & -\sin\gamma \\ \frac{\sin\beta\sin\gamma}{\cos\beta} & 1 & \frac{\sin\beta\cos\gamma}{\cos\beta} \end{bmatrix}.$$

The inverse of $\Phi(\eta)$ is $\Psi = \Phi^{-1}$, which is given by

$$\Psi(\eta) = \begin{bmatrix} \cos\beta\sin\gamma & \cos\gamma & 0 \\ -\sin\beta & 0 & 1 \\ \cos\beta\cos\gamma & -\sin\gamma & 0 \end{bmatrix}.$$

The dynamics of the translational motion is given by

$$m\ddot{p} + mge_3 + \lambda_1 A^T + \lambda_2 e_1 = Rfe_3 \tag{4}$$

where λ_1 is the term about side slipping, λ_2 is the term about the force to push the drone against the wall, and

$$A = [0 \ r_{22} \ r_{32}].$$

The dynamics of the rotational motion [22] is given by

$$M(\eta)\ddot{\eta} + C(\eta,\dot{\eta})\dot{\eta} = \Psi(\eta)^T\tau^b - \lambda_3 e_1 \tag{5}$$

where λ_3 is the term about yawing and

$$M(\eta) = \Psi(\eta)^T J\Psi(\eta)$$
$$C(\eta,\dot{\eta}) = \Psi(\eta)^T J\dot{\Psi}(\eta) + \Psi(\eta)\mathrm{sk}(\Psi(\eta)\dot{\eta})J\Psi(\eta).$$

2.2. Exponential control barrier functions(ECBF)

CBF can be applied when the derivative of $h(x)$ is one. We relax this relative degree condition and assume that $h(x)$ has a higher relative degree $r \geq 1$, i.e., it satisfies the following equation,

$$h^{(r)}(x,u) = L_f^r h(x) + L_g L_f^{r-1} h(x)u.$$

Here, $L_g L_f^{r-1} h(x) \neq 0$ and $L_g L_f^2 h(x) = \cdots \ L_g L_f^{r-2} h(x) = 0$, $\forall x \in D$

Definition 2.1. [13] Given a set $C \subset D \subset \mathbb{R}$, a function $h : D \to \mathbb{R}$ that is r times continuously differentiable is an exponential control barrier function(ECBF) if there

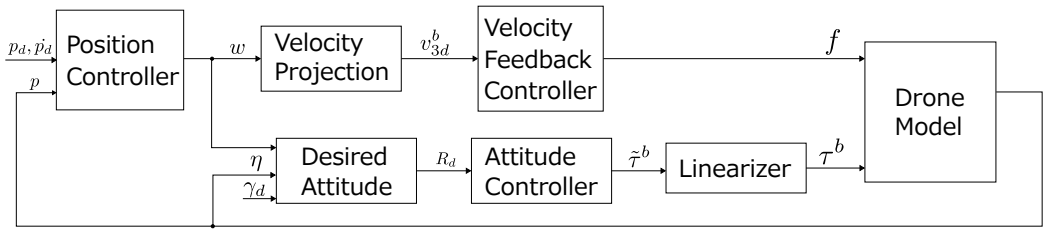

Figure 2. Block diagram of the proposed control structure.

exists a column vector $K_\alpha \in \mathbb{R}^r$ that satisfies the following equation for all $x \in D$,

$$\sup_{u \in U}[L_f^r h(x) + L_g L_f^{r-1} h(x) u] \geq -K_\alpha \eta_b(x).$$

Here, $\forall x \in \mathrm{Int}(C)$, $h(x(t)) \geq Ce^{(F-GK_\alpha)t}\eta_b(x_0)$ whenever $h(x_0) \geq 0$.

3. Control design

In this section, we design the control law of trajectory tracking for the two-wheeled drone. The control structure of this paper is shown in Fig. 2. We design the control law of translational motion based on kinematics. Therefore, we design the velocity feedback control law for velocity projection, and by using this, we finally get the thrust. Furthermore, we design the control law of rotational motion based on linearized dynamics.

3.1. Velocity input design

In this paper, we propose a trajectory tracking control law for two-wheeled drones based on the control law for unicycle mobile robots [9]. Suppose that the position y, z of the drone is $X = [y\ z]^T \in \mathbb{R}^2$, the target position of y, z is $X_d = [y_d\ z_d]^T \in \mathbb{R}^2$, the position error of y, z is $\tilde{X} = [y - y_d\ z - z_d]^T = X - X_d \in \mathbb{R}^2$, $v_3^b = v_{3d}^b$, and the positive definite matrix $K_p > 0$. From (2) and (3), the yz translation kinematics and roll kinemtics is given by the following equation,

$$\dot{p} = \frac{1}{\cos\gamma} \begin{bmatrix} \cos\beta & -\sin\beta \\ \sin\beta & \cos\beta \end{bmatrix} \begin{bmatrix} 0 \\ v_{3d}^b \end{bmatrix} \tag{6}$$

$$\dot{\beta} = r_\beta.$$

Considering the nonholonomic constraint $v_2^b = 0$, the desired velocity w is transformed into the projection velocity by the following equation,

$$v_{3d}^b = w^T \left(E^T R_2(\beta) E\right)\left(E^T e_3\right) \tag{7}$$

where $E = [e_2\ e_3] \in \mathbb{R}^{3\times 2}$. Then, the desired velocity $w = [w_y\ w_z] \in \mathbb{R}^2$ is designed by the following translational controller,

$$w = \cos\gamma_d(-K_p\tilde{X} + \dot{X}_d). \tag{8}$$

Furthermore, the roll controller is given by the following equation,

$$r_\beta = r_{\beta_d} - k_R(\mathrm{sk}(\tilde{R}))^\vee \tag{9}$$

where

$$\begin{cases} \tilde{R} & = R_d^T E^T R_2(\beta) E \\ R_d & = \left[(-1)^\wedge \frac{w}{\|w\|}\ \ \frac{w}{\|w\|}\right] \\ r_{\beta_d} & = (R_d^T \dot{R}_d)^\vee. \end{cases}$$

Therefore, the following theorem holds.

Theorem 3.1. *Consider the two-wheeled drone kinematics* (6), (3) *in closed-loop with the controllers* (8), (7), *and* (9), *and assume* $v_3^b = v_{3d}^b$. *Then, the origin of the system is almost global asymptotically stable.*

Proof. The proof is same as [9]. □

From here, we extend Theorem 3.1 to the entire system of two-wheeled drones.

3.2. Linearlization of rotational dynamics and pitch controller

We define a new virtual input $\tilde{\tau}^b \in \mathbb{R}^3$ as follows,

$$\tau^b = J\Psi(\eta)\tilde{\tau}^b + \left(\Psi(\eta)^T\right)^{-1} C(\eta,\dot{\eta})\dot{\eta} + \lambda_3 e_1.$$

Then, the rotational dynamics (5) can be linearized as follows,

$$\ddot{\eta} = \tilde{\tau}^b. \tag{10}$$

When running on the wall, it is important for two-wheeled drones to push the drone against the wall. This is because the stability of the drone against sideslip or side wind is increased and the grip is improved. By (10), the linearized dynamics of the pitch direction is given by the following equation,

$$\ddot{\gamma} = \tilde{\tau}_\gamma^b. \tag{11}$$

We design the pitch controller as follows,

$$\tilde{\tau}_\gamma^b = -k_{p_\gamma}(\gamma - \gamma_d) - k_{d_\gamma}(\dot{\gamma} - \dot{\gamma}_d) \tag{12}$$

where $k_{p_\gamma}, k_{d_\gamma} > 0$.

3.3. Roll controller

The linearized dynamics of the roll is given by the following equation,

$$\ddot{\beta} = \tilde{\tau}_{\beta}^{b}. \tag{13}$$

Then, the roll controller for (13) is given by the following equation,

$$\tilde{\tau}_{\beta}^{b} = -k_{\beta}(\dot{\beta} - r_{\beta}) + \dot{r}_{\beta} \tag{14}$$

where $k_{\beta} > 0$.

3.4. Translational dynamics and velocity feedback

We design the controller to obtain the thrust from the velocity projection v_{3d}^{b} obtained by the translational controller. (4) and (2) give the following equation,

$$f = m(f_1 \dot{v}_3^b + f_2 + f_3)$$

where

$$\begin{cases} f_1 &= 1 - \frac{r_{13}(r_{32}r_{21} - r_{22}r_{31})}{r_{11}(r_{32}r_{23} - r_{22}r_{33})} \\ f_2 &= \frac{v_3^b \omega_2^b (r_{32}r_{21} - r_{22}r_{31} - r_{11}) - g r_{11} r_{22} + \omega_2^b r_{13} v_1^b}{r_{11}(r_{32}r_{23} - r_{22}r_{33})} \\ f_3 &= v_1^b \omega_2^b. \end{cases}$$

Therefore, the velocity feedback control law $\dot{v}_3^b = -k_3(v_3^b - v_{3d}^b) + \dot{v}_{3d}^b$ is applied by the positive constant $k_3 > 0$. Then, the thrust is given by the following equation,

$$f = m\left(f_1\left(-k_3\left(v_3^b - v_{3d}^b\right) + \dot{v}_{3d}^b\right) + f_2 + f_3\right).$$

Hence, the main theorem of the stability in this paper is obtained as follows.

Theorem 3.2. *Consider the closed-loop system of the kinematics* (2), (3), *and the dynamics* (4), (5) *of the two-wheeled drones with the controller* (8), (12), *and* (14). *Then, the equilibrium points* $p_e = 0$, $\tilde{R} = I$, *and* $\gamma_e = 0$ *are almost global asymptotically stable.*

Proof. From (2), the yz kinematics of the translational motion is given by the following equation,

$$\begin{aligned} \dot{X} &= \frac{1}{\cos\gamma}(v_{3d}^b - \tilde{v}_3^b)(E^T R_2(\beta) E)(E^T e_3) \\ &= \frac{v_{3d}^b}{\cos\gamma_d}(E^T R_2(\beta) E)(E^T e_3) + \Delta_2 + \Delta_3 \end{aligned}$$

where $\tilde{v}_3^b = v_{3d}^b - v_3^b$ and

$$\Delta_2 = -\frac{v_{3d}^b}{\cos\gamma_d}(E^T R_2(\beta)E)(E^T e_3) + \frac{v_{3d}^b}{\cos\gamma}(E^T R_2(\beta)E)(E^T e_3)$$

$$\Delta_3 = -\frac{\tilde{v}_3^b}{\cos\gamma}(E^T R_2(\beta)E)(E^T e_3).$$

From (13) and (14), the linearized dynamics of the roll direction is given by the following equation,

$$\ddot{\beta} = -k_\beta(\dot{\beta} - r_\beta) + \dot{r}_\beta. \tag{15}$$

(15) can be rewritten as follows,

$$\ddot{\beta}_e = -k_\beta \dot{\beta}_e \tag{16}$$

where $\dot{\beta}_e = \dot{\beta} - r_\beta$. Therefore, the system (16) is asymptotically stable. (15) can be rewritten as follows,

$$\ddot{\beta} = \Delta_1 + \dot{r}_\beta \tag{17}$$

where $\Delta_1 = -k_\beta(\dot{\beta} - r_\beta)$. Furthermore, by integrating both sides of (17), we get the following equation,

$$\dot{\beta}(t) = \int_{t_0}^{t} \ddot{\beta}(\tau)d\tau + \dot{\beta}(t_0) = \Delta_1' + r_\beta(t) - r_\beta(t_0) + \dot{\beta}(t_0) \tag{18}$$

where $\Delta_1' = \int_{t_0}^{t} \Delta_1 d\tau$. By writing (18) as $SO(2)$, we get the following equation,

$$\dot{R} = R\begin{bmatrix} 0 & -\dot{\beta}(t) \\ \dot{\beta}(t) & 0 \end{bmatrix} = R\begin{bmatrix} 0 & -r_\beta(t) \\ r_\beta(t) & 0 \end{bmatrix} + \Delta_1'' \tag{19}$$

where

$$\Delta_1'' = R\begin{bmatrix} 0 & -(\Delta_1' + r_\beta(t) - r_\beta(t_0) + \dot{\beta}(t_0)) \\ \Delta_1' + r_\beta(t) - r_\beta(t_0) + \dot{\beta}(t_0) & 0 \end{bmatrix}.$$

Furthermore, (19) can be rewritten to the error system as follows,

$$\dot{\tilde{R}} = \tilde{R}\hat{\tilde{r}}_\beta(t) + \Delta_1'''$$

where $\tilde{r}_\beta = r_\beta - r_{\beta_d}$. From (11) and (12), the linearized dynamics of the pitch direction

is given by the following equation,

$$\ddot{\gamma} - \ddot{\gamma}_d = -k_{p_\gamma}(\gamma - \gamma_d) - k_{d_\gamma}(\dot{\gamma} - \dot{\gamma}_d) \tag{20}$$

(20) can be rewritten as follows,

$$\ddot{\gamma}_e = -k_{p_\gamma}\gamma_e - k_{d_\gamma}\dot{\gamma}_e \tag{21}$$

where $\gamma_e = \gamma - \gamma_d$. Therefore, (21) is rewritten as follows,

$$\frac{d}{dt}\begin{bmatrix}\gamma_e \\ \dot{\gamma}_e\end{bmatrix} = \begin{bmatrix}0 & 1 \\ -k_{p_\gamma} & -k_{d_\gamma}\end{bmatrix}\begin{bmatrix}\gamma_e \\ \dot{\gamma}_e\end{bmatrix}. \tag{22}$$

The closed-loop system of the two-wheeled drone is given by the following equation,

$$\begin{cases} \dot{\tilde{X}} & = -K_p\tilde{X} + \|K_p\tilde{X} + \dot{X}_d\|\left(\left(\left(E^T e_3\right)^T \tilde{R}\right) R_d\tilde{R}(E^T e_3) - R_d(E^T e_3)\right) + \Delta_2 + \Delta_3 \\ \dot{\tilde{R}} & = -k_R\tilde{R}\mathrm{sk}(\tilde{R}) + \Delta_1''' \\ \frac{d}{dt}\begin{bmatrix}\gamma_e \\ \dot{\gamma}_e\end{bmatrix} & = \begin{bmatrix}0 & 1 \\ -k_{p_\gamma} & -k_{d_\gamma}\end{bmatrix}\begin{bmatrix}\gamma_e \\ \dot{\gamma}_e\end{bmatrix}. \end{cases}$$

From (22), the equilibrium point $\gamma_e = 0$ is global asymptotically stable. From (14), $\dot{\beta}$ converges to r_β, so Δ_1' converges to 0. Furthermore, γ converges to γ_d, so Δ_2 converges to 0. Furthermore, v_3^b converges to v_{3d}^b, so Δ_3 converges to 0. For these reasons, the equilibrium point $p_e = 0$, $\tilde{R} = I$, and $\gamma_e = 0$ is almost global asymptotically stable. □

4. Control design using control barrier functions

In this section, we design ECBF-QP to avoid obstacles considering sideslipping.

4.1. Problem settings and program formulation

Consider a two-wheeled drone moving on a wall with a circular obstacle of a center $p_c = [0, y_c, z_c]^T$ and a radius $r \in \mathbb{R}$. We show the outline drawing of the control law of this paper in Fig. 3. The blue dotted line is the image of the target trajectory, and the green solid line is the image of the trajectory when the obstacle avoidance control is used. When the target trajectory is inside the obstacle, it is necessary to avoid the obstacle. However, if the drone tries to avoid the obstacle by rolling on the wall, the gravity component in the lateral direction becomes large, and there is a risk of slipping. Therefore, the control objective of this paper is to avoid obstacles without slipping. The condition for not slipping is expressed by the following equation,

$$\|\lambda_1 A^T\| \leq \mu\|\lambda_2 e_1\|. \tag{23}$$

where coefficient of static friction is $\mu \in \mathbb{R}$, slipping force is $\|\lambda_1 A^T\|$, and pushing force to the wall is $\|\lambda_2 e_1\|$. $A^T = [0\ r_{22}\ r_{32}]^T$ gives $\|A^T\| = 1$ and since $\|\lambda_2 e_1\|$ is pushing

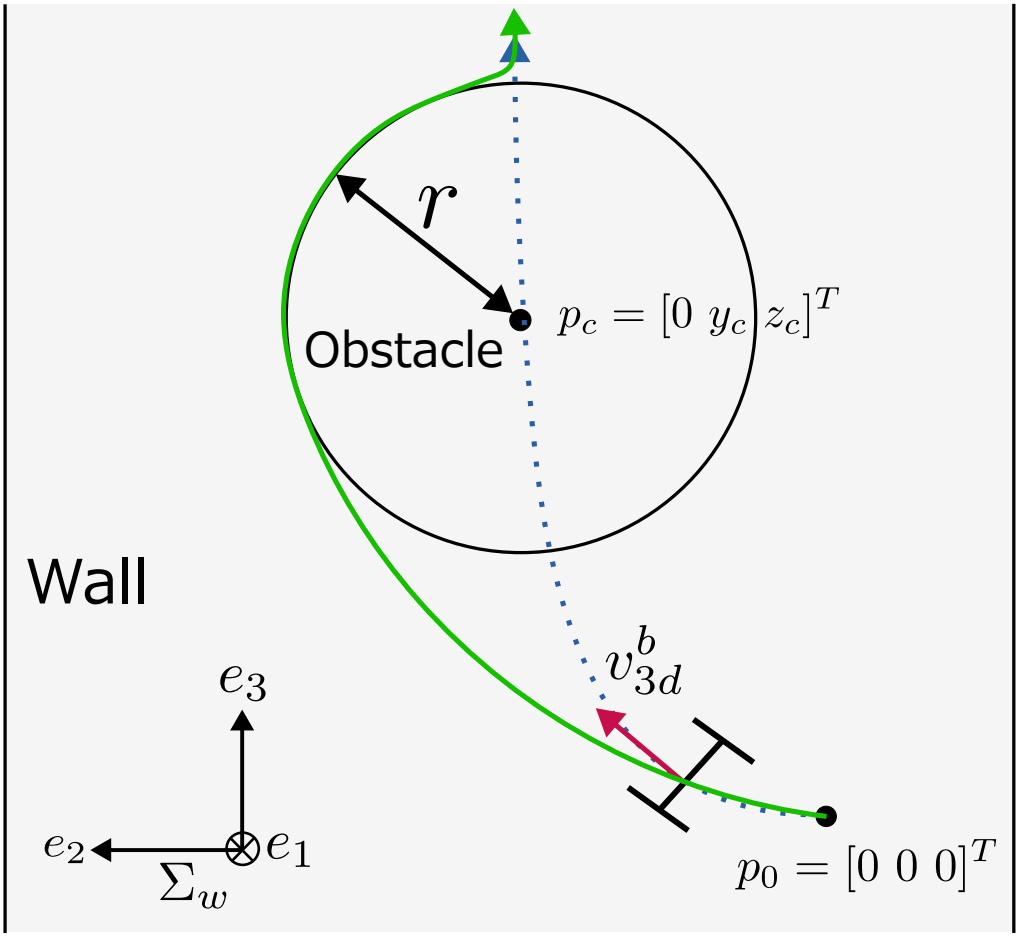

Figure 3. Outline drawing of obstacle avoidance.

force, $\lambda_2 \geq 0$. Therefore, we can transform the equation (23) as follows,

$$\|\lambda_1\| \leq \mu\lambda_2. \tag{24}$$

Hence, the control objective of this paper is to design the input f, τ^b that satisfies the condition (24) and the following equation,

$$\begin{cases} \lim\limits_{t\to\infty} \|p - p_d\| = 0 & \text{if } \|p_d - p_c\| > r \\ \|p - p_c\| \geq r & \text{otherwise.} \end{cases}$$

The control structure of the ECBF-QP combined with obstacle avoidance and sideslip is shown in Fig. 4. The constraint equation of ECBF-QP for obstacle avoidance contains $\tilde{\tau}_\beta^b$, but doesn't contain $\tilde{\tau}_\gamma^b$. On the other hand, the constraint equation of ECBF-QP for sideslip contain both $\tilde{\tau}_\beta^b$ and $\tilde{\tau}_\gamma^b$. Therefore, the linearized roll torque $\tilde{\tau}_\beta^b$ is modified by the ECBF-QP for obstacle avoidance, and then, the linearized pitch torque $\tilde{\tau}_\gamma^b$ is modified by the ECBF-QP for sideslip.

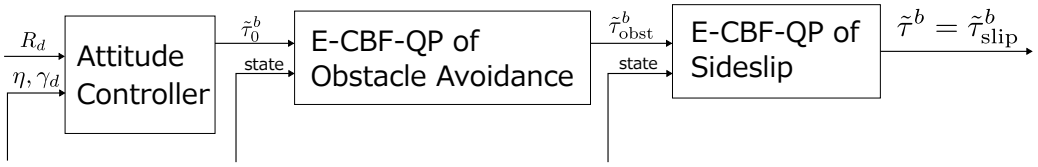

Figure 4. Control structure of ECBF-QP.

4.2. Control design of ECBF-QP for obstacle avoidance

We consider the control barrier function as follows,

$$h_{\text{obst}} = (y - y_c)^2 + (z - z_c)^2 - r^2.$$

We consider the linearized roll torque $\tilde{\tau}_\beta^b$ as an input. Therefore, $\dddot{h}_{\text{obst}} + \alpha_1 h_{\text{obst}} + \alpha_2 \dot{h}_{\text{obst}} + \alpha_3 \ddot{h}_{\text{obst}} \geq 0$ can be written as follows,

$$f_x + g_x \tilde{\tau}_\beta^b \leq 0$$

where f_x, g_x can be obtained by Symbolic Math Toolbox in MATLAB, especially g_x is as follows,

$$\begin{aligned} g_x = 2\left((z_c - z)\sin\beta + (y_c - y)\cos\beta\right) \\ \times(-\cos\beta\dot{z} + \sin\beta\dot{y}). \end{aligned}$$

Hence, ECBF-QP for obstacle avoidance is obtained as follows,

$$\begin{cases} \tilde{\tau}_{\text{obst}}^b = \underset{\tilde{\tau}_{\text{obst}}^b \in \mathbb{R}}{\arg\min} \|\tilde{\tau}_{\text{obst}}^b - \tilde{\tau}_0^b\|^2 \\ \text{s.t.} \quad f_x + g_x \tilde{\tau}_\beta^b \leq 0. \end{cases}$$

4.3. Control design of ECBF-QP for sideslip

When avoiding obstacles, two-wheeled drones need to roll, so sideslip is likely to occur. For HyTAQs, there is research on considering sideslipping during ground running [23]. In this chapter, we design a control barrier function to avoid sideslip in addition to the control barrier function for obstacle avoidance and consider the linearized pitch toqrue $\tilde{\tau}_\gamma^b$ as an input.

Condition not to sideslip can be written as follows,

$$f_{\text{slip}} \leq \mu N \tag{25}$$

where f_{slip} is the force to make the drone sideslip, N is the force to push the drone against the wall, and μ is the coefficient of static friction. The force to make the drone sideslip is $\|\lambda_1 A^T\|$, and the force to push the drone against the wall is $\|\lambda_2 e_1\|$, so (25) can be written as follows,

$$\|\lambda_1 A^T\| \leq \mu \|\lambda_2 e_1\|. \tag{26}$$

λ_1 can take both positive and negative values, but $\lambda_2 \geq 0$, and $\|A^T\| = 1$ and $\|e_1\| = 1$, so (26) can be written as follows,

$$\|\lambda_1\| \leq \mu\lambda_2. \tag{27}$$

The inequality (27) is an inequality containing absolute values, so we consider the conditions by dividing the cases.

If $\lambda_1 \geq 0$, (27) can be written as follows,

$$mg\sin\beta + f\mu\sin\gamma - m\cos\beta\dot{z}\dot{\beta} + m\sin\beta\dot{y}\dot{\beta} \geq 0.$$

Therefore, the control barrier function h_{slip_1} can be defined as follows,

$$\begin{aligned} h_{\text{slip}_1} \coloneqq\ & mg\sin\beta + f\mu\sin\gamma \\ & -m\cos\beta\dot{z}\dot{\beta} + m\sin\beta\dot{y}\dot{\beta}. \end{aligned} \tag{28}$$

(28) is a function of $\tilde{\tau}_\gamma^b$ in the second order, so the relative degree is 2. Therefore, $\ddot{h}_{\text{slip}_1} + \alpha_4\dot{h}_{\text{slip}_1} + \alpha_5\dot{h}_{\text{slip}_1} \geq 0$ can be written as follows,

$$f_x + g_x\tilde{\tau}_\gamma^b \leq 0$$

where f_x, g_x can be obtained by Symbolic Math Toolbox in MATLAB, especially g_x is as follows,

$$g_x = -\mu\cos\gamma f.$$

If $\lambda_1 < 0$, the control barrier function h_{slip_2} can be defined as follows similar to $\lambda_1 \geq 0$,

$$\begin{aligned} h_{\text{slip}_2} \coloneqq\ & f\mu\sin\gamma - mg\sin\beta \\ & +m\cos\beta\dot{z}\dot{\beta} - m\sin\beta\dot{y}\dot{\beta}. \end{aligned}$$

Therefore, $\ddot{h}_{\text{slip}_2} + \alpha_4\dot{h}_{\text{slip}_2} + \alpha_5\dot{h}_{\text{slip}_2} \geq 0$ can be written as follows,

$$f_x + g_x\tilde{\tau}_\gamma^b \leq 0$$

where f_x, g_x can be obtained by Symbolic Math Toolbox in MATLAB, especially g_x is as follows,

$$g_x = -\mu\cos\gamma f.$$

Hence, ECBF-QP for sideslip is obtained as follows,

$$\begin{cases} \tilde{\tau}_{\text{slip}}^b = \underset{\tilde{\tau}_{\text{slip}}^b \in \mathbb{R}}{\arg\min} \|\tilde{\tau}_{\text{slip}}^b - \tilde{\tau}_{\text{obst}}^b\|^2 \\ \text{s.t.} \quad f_x + g_x\tilde{\tau}_\gamma^b \leq 0. \end{cases}$$

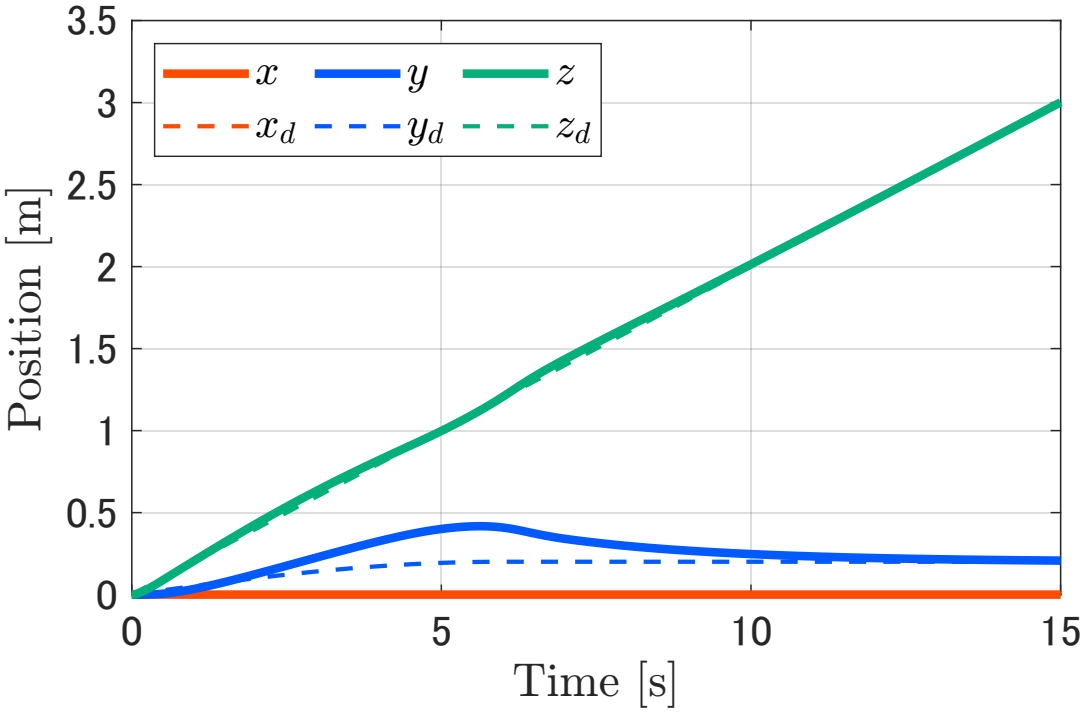

Figure 5. Simulation result of position.

5. Simulation condition and results

In this chapter, we verify that the control objectives are achieved by simulation of the control design in this paper. We consider $m = 0.938\text{kg}$, $J = \text{diag}[0.00933\ 0.00285\ 0.01130]\text{kg}\,\text{m}^2$, $g = 9.81\text{m/s}^2$ as the physical parameters of the two-wheeled drone. We also consider $k_3 = 10$ as the velocity feedback gain, $K_p = \text{diag}([0.5, 0.5, 0.5])$ as the position controller, $k_R = 4$, $k_\beta = 2$, $k_{p_\gamma} = 5$, $k_{d_\gamma} = 5$ as the attitude controller and $[y_c\ z_c] = [-0.2\ 1.0]\text{m}$, $r = 0.5\text{m}$, $\alpha_1 = 0.4$, $\alpha_2 = 0.3$, $\alpha_3 = 0.3$ as the parameters of the ECBF-QP for obstacle avoidance, and $\mu = 0.5$, $\alpha_4 = 20$, $\alpha_5 = 10$ as the parameters of the ECBF-QP for avoiding sideslip. Furthermore, the initial values are $p_0 = [0\ 0\ 0]^T\text{m}$, $\dot{p}_0 = [0\ 0\ 0]^T\text{m/s}$, $\eta_0 = [0\ 0\ \frac{5\pi}{180}]^T\text{rad}$, $\dot{\eta}_0 = [0\ 0\ 0]^T\text{rad/s}$, the target value is $\gamma_d = \frac{15\pi}{180}\text{rad}$, and the target trajectory on the wall p_d is given by the following equation,

$$p_d = \begin{bmatrix} 0 \\ 0.2\sin\frac{15\pi}{180}t\ (0 \le t < 6), \quad 0.2\ (6 \le t) \\ 0.2t \end{bmatrix}.$$

We show the simulation results of the position, attitude, thrust, and torque in Fig. 5, Fig. 6, Fig. 7, Fig. 8, respectively. We also show the animation of the simulation result in Fig. 9 and the trajectory on the wall in Fig. 10. From Fig. 5, Fig. 10. We can see that the two-wheeled drone avoids the obstacle and follows the target trajectory. Furthermore, we show the control barrier functions for obstacle avoidance and sideslip in Fig. 11, Fig. 12, respectively. The control barrier function for sideslip is defined by

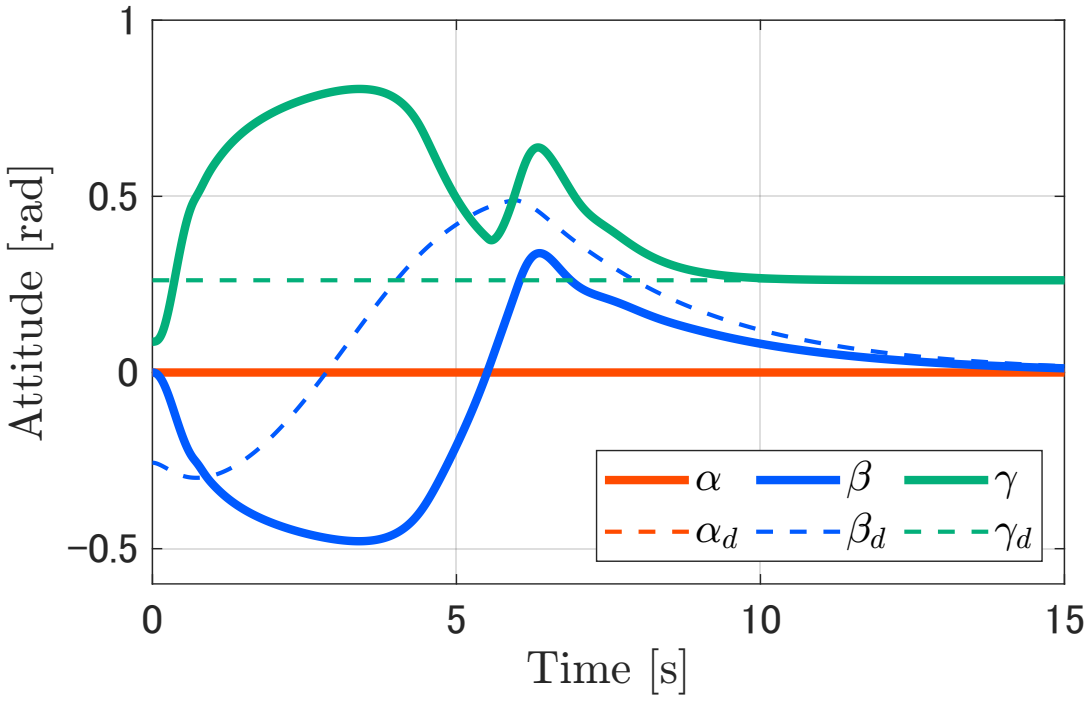

Figure 6. Simulation result of attitude.

the following equation,

$$h_{\text{slip}} = \begin{cases} h_{\text{slip}_1} & (\lambda_1 \geq 0), \\ h_{\text{slip}_2} & (\lambda_1 < 0). \end{cases}$$

From Fig. 11, we can see that $h_{\text{obst}} \geq 0$, and from Fig. 12, we can see that $h_{\text{slip}} \geq 0$. Therefore, the two-wheeled drone satisfies the constraints of obstacle avoidance and sideslip.

6. Conclusion

In this paper, we proposed an obstacle avoidance control for two-wheeled drones considering sideslip based on control barrier functions. First, we derived the ZXY Euler angle-based Lagrange equation of them on a wall.

Next, we extended [9] and designed a control law for trajectory tracking of two-wheeled drones on a wall, and proved that the origin of the system is almost globally asymptotically stable.

Furthermore, we designed ECBF-QP for obstacle avoidance and sideslip using control barrier functions, and combined them.

Finally, we confirmed the effectiveness of the proposed control law for two-wheeled drones by numerical simulations.

As a future work, we will compare the $SE(2)$-based control law for two-wheeled drones in [24] and the trajectory tracking control law in this paper, and consider the solvability conditions of CBF-QP.

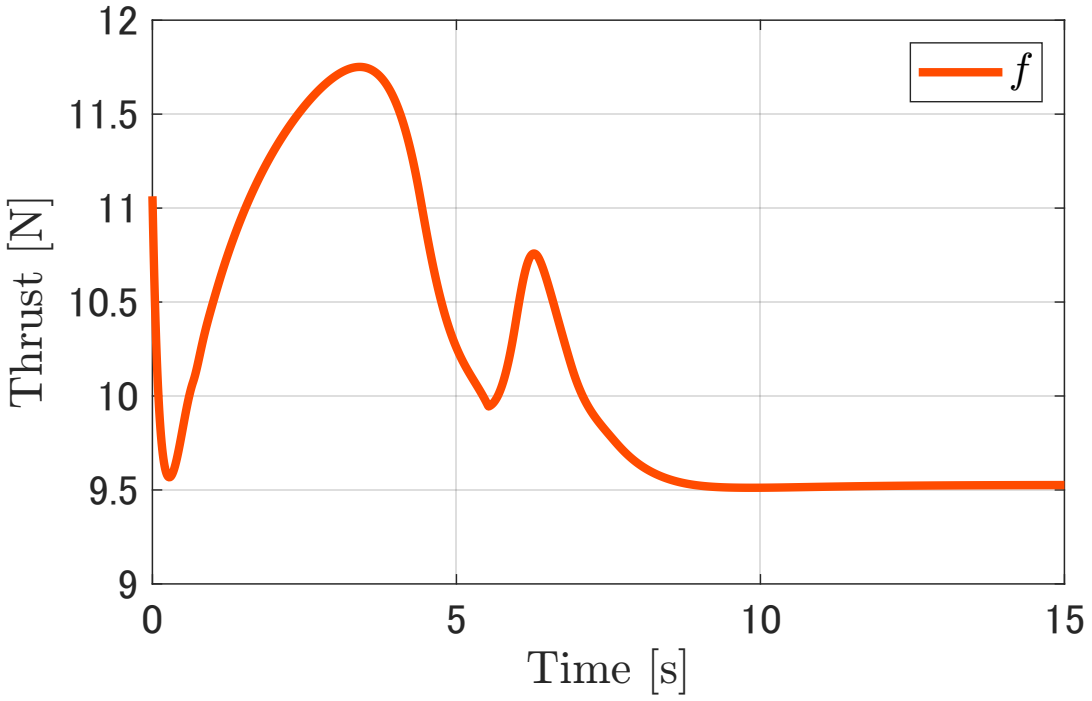

Figure 7. Simulation result of thrust.

References

[1] Kooijman D, Schoellig AP, Antunes DJ. Trajectory Tracking for Quadrotors with Attitude Control on $\mathcal{S}^2 \times \mathcal{S}^1$. In: 2019 18th European Control Conference (ECC); Jun.; Naples, Italy. IEEE; 2019. p. 4002–4009.

[2] Lee T, Leok M, McClamroch NH. Control of Complex Maneuvers for a Quadrotor UAV Using Geometric Methods on $SE(3)$; 2011.

[3] Lee T, Leok M, McClamroch NH. Geometric Tracking Control of a Quadrotor UAV on $SE(3)$. In: 49th IEEE Conference on Decision and Control (CDC); Dec.; Atlanta, GA. IEEE; 2010. p. 5420–5425.

[4] Fan DD, Thakker R, Bartlett T, et al. Autonomous Hybrid Ground/Aerial Mobility in Unknown Environments. In: 2019 IEEE/RSJ International Conference on Intelligent Robots and Systems (IROS); Nov.; Macau, China. IEEE; 2019. p. 3070–3077.

[5] Kalantari A, Spenko M. Design and experimental validation of HyTAQ, a Hybrid Terrestrial and Aerial Quadrotor. In: 2013 IEEE International Conference on Robotics and Automation; May; Karlsruhe, Germany. IEEE; 2013. p. 4445–4450.

[6] Wu T, Zhu Y, Zhang L, et al. Motion Planning for HyTAQs: A Topology-guided Unified NMPC Approach. In: 2022 IEEE/RSJ International Conference on Intelligent Robots and Systems (IROS); Oct.; Kyoto, Japan. IEEE; 2022. p. 4835–4840.

[7] W BR. Asymptotic Stability and Feedback Stabilization. Differential Geometric Control Theory. 1983;27:181–191. Available from: `https://cir.nii.ac.jp/crid/1572824499073211520`.

[8] Bhat SP, Bernstein DS. A Topological Obstruction to Continuous Global Stabilization of Rotational Motion and the Unwinding Phenomenon. Systems & Control Letters. 2000; 39(1):63–70. Available from: `https://www.sciencedirect.com/science/article/pii/S0167691199000900`.

[9] Rodríguez-Cortés H, Velasco-Villa M. A New Geometric Trajectory Tracking Controller for the Unicycle Mobile Robot. Systems & Control Letters. 2022 Oct;168:105360.

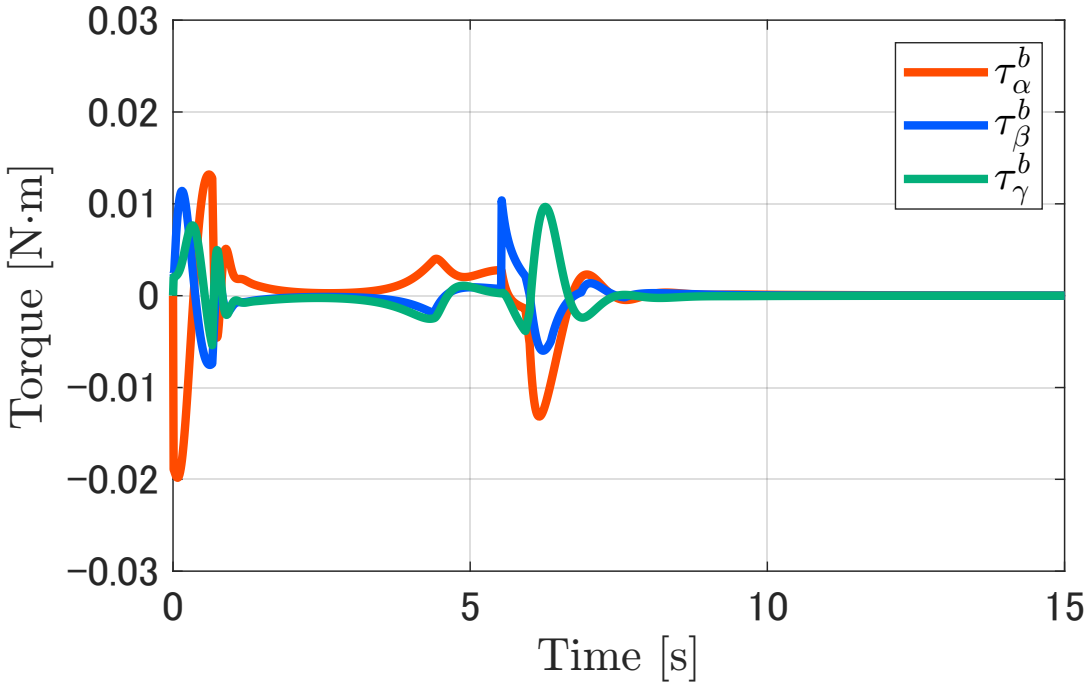

Figure 8. Simulation result of torque.

[10] Lee T, Leok M, McClamroch NH. Nonlinear Robust Tracking Control of a Quadrotor UAV on $SE(3)$. Asian Journal of Control. 2013;15(2):391–408. Available from: `https://onlinelibrary.wiley.com/doi/abs/10.1002/asjc.567`.

[11] Angeli D. Almost Global Stabilization of the Inverted Pendulum via Continuous State Feedback. Automatica. 2001;37(7):1103–1108. Available from: `https://www.sciencedirect.com/science/article/pii/S0005109801000644`.

[12] Ames AD, Xu X, Grizzle JW, et al. Control Barrier Function Based Quadratic Programs for Safety Critical Systems. IEEE Transactions on Automatic Control. 2017 Aug; 62(8):3861–3876.

[13] Ames AD, Coogan S, Egerstedt M, et al. Control Barrier Functions: Theory and Applications. In: 2019 18th European Control Conference (ECC); Jun.; Naples, Italy. IEEE; 2019. p. 3420–3431.

[14] Huang Y, Yong SZ, Chen Y. Guaranteed Vehicle Safety Control Using Control-Dependent Barrier Functions. In: 2019 American Control Conference (ACC); Jul.; Philadelphia, PA, USA. IEEE; 2019. p. 983–988.

[15] Li B, Wen S, Yan Z, et al. A Survey on the Control Lyapunov Function and Control Barrier Function for Nonlinear-Affine Control Systems. IEEE/CAA Journal of Automatica Sinica. 2023 Mar;10(3):584–602.

[16] Ames AD, Grizzle JW, Tabuada P. Control Barrier Function Based Quadratic Programs with Application to Adaptive Cruise Control. In: 53rd IEEE Conference on Decision and Control; Dec.; Los Angeles, CA, USA. IEEE; 2014. p. 6271–6278.

[17] Xiao W, Belta C. Control Barrier Functions for Systems with High Relative Degree. In: 2019 IEEE 58th Conference on Decision and Control (CDC); Dec.; Nice, France. IEEE; 2019. p. 474–479.

[18] Desai M, Ghaffari A. CLF-CBF Based Quadratic Programs for Safe Motion Control of Nonholonomic Mobile Robots in Presence of Moving Obstacles. In: 2022 IEEE/ASME International Conference on Advanced Intelligent Mechatronics (AIM); Jul.; Sapporo, Japan. IEEE; 2022. p. 16–21.

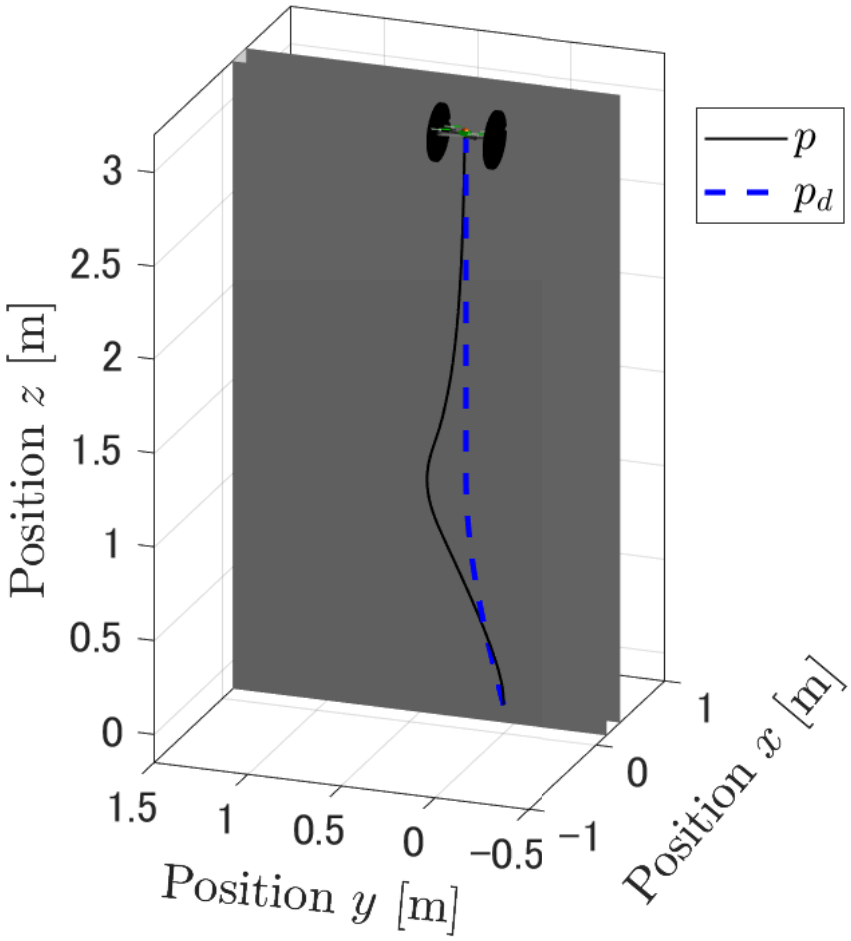

Figure 9. Animation of the simulation result.

[19] Marley M, Skjetne R, Teel AR. Synergistic control barrier functions with application to obstacle avoidance for nonholonomic vehicles. In: 2021 American Control Conference (ACC); May; New Orleans, LA, USA. IEEE; 2021. p. 243–249.

[20] Khan M, Zafar M, Chatterjee A. Barrier Functions in Cascaded Controller: Safe Quadrotor Control. In: 2020 American Control Conference (ACC); Jul.; Denver, CO, USA. IEEE; 2020. p. 1737–1742.

[21] Wu G, Sreenath K. Safety-Critical Control of a Planar Quadrotor. In: 2016 American Control Conference (ACC); Jul.; Boston, MA, USA. IEEE; 2016. p. 2252–2258.

[22] Nonami K, Kendoul F, Suzuki S, et al., editors. Autonomous Flying Robots: Unmanned Aerial Vehicles and Micro Aerial Vehicles. Tokyo ; New York: Springer; 2010. OCLC: ocn471803402.

[23] Wu T, Zhu Y, Zhang L, et al. Unified Terrestrial/Aerial Motion Planning for HyTAQs via NMPC. IEEE Robotics and Automation Letters. 2023 Feb;8(2):1085–1092.

[24] Tayefi M, Geng Z. Logarithmic Control, Trajectory Tracking, and Formation for Nonholonomic Vehicles on Lie Group $SE(2)$. International Journal of Control. 2017 06;92.

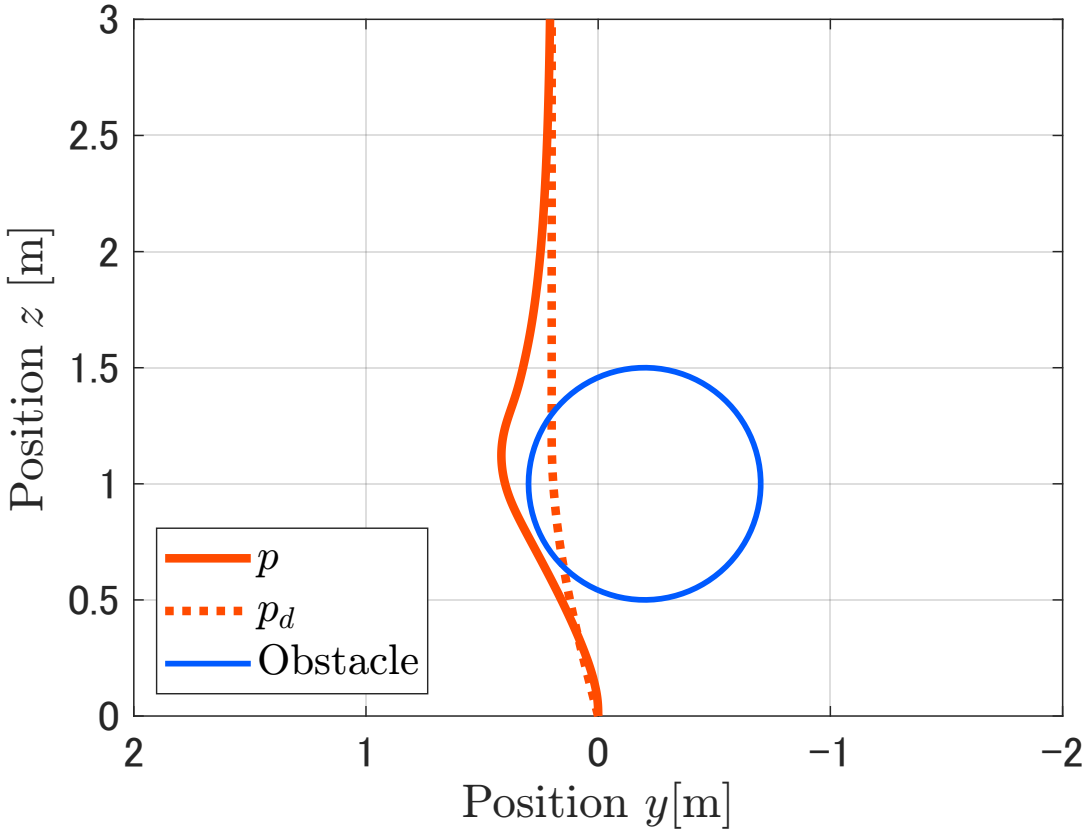

Figure 10. Trajectory of the simulation result.

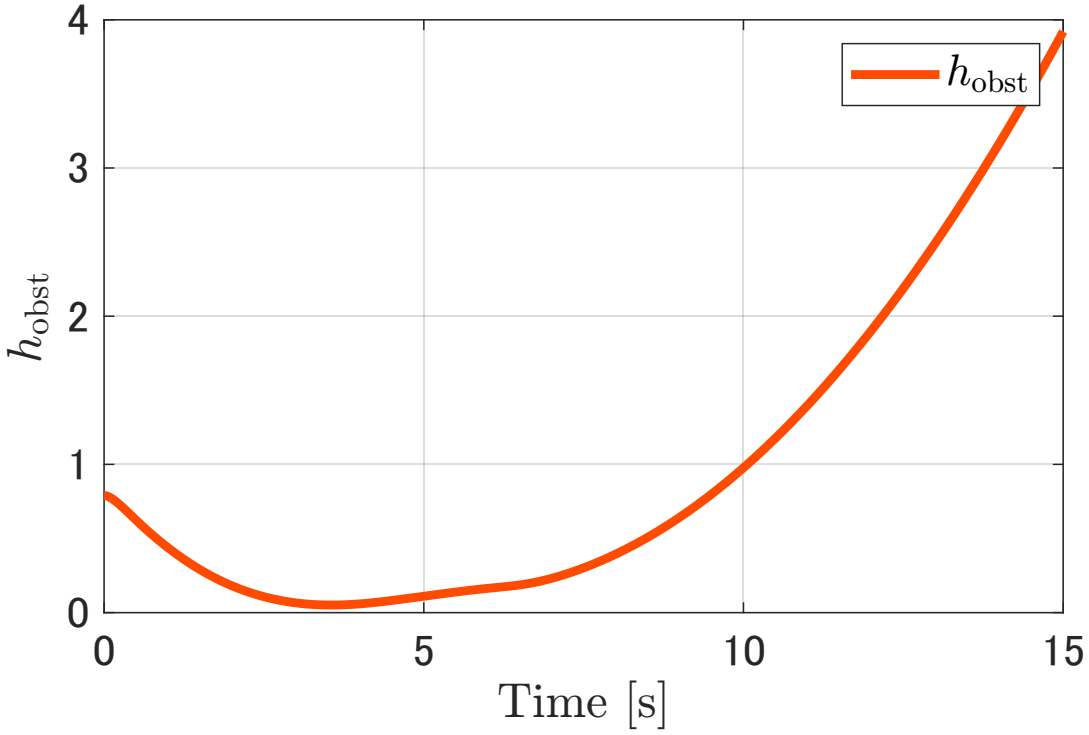

Figure 11. Obstacle CBF of the simulation result.

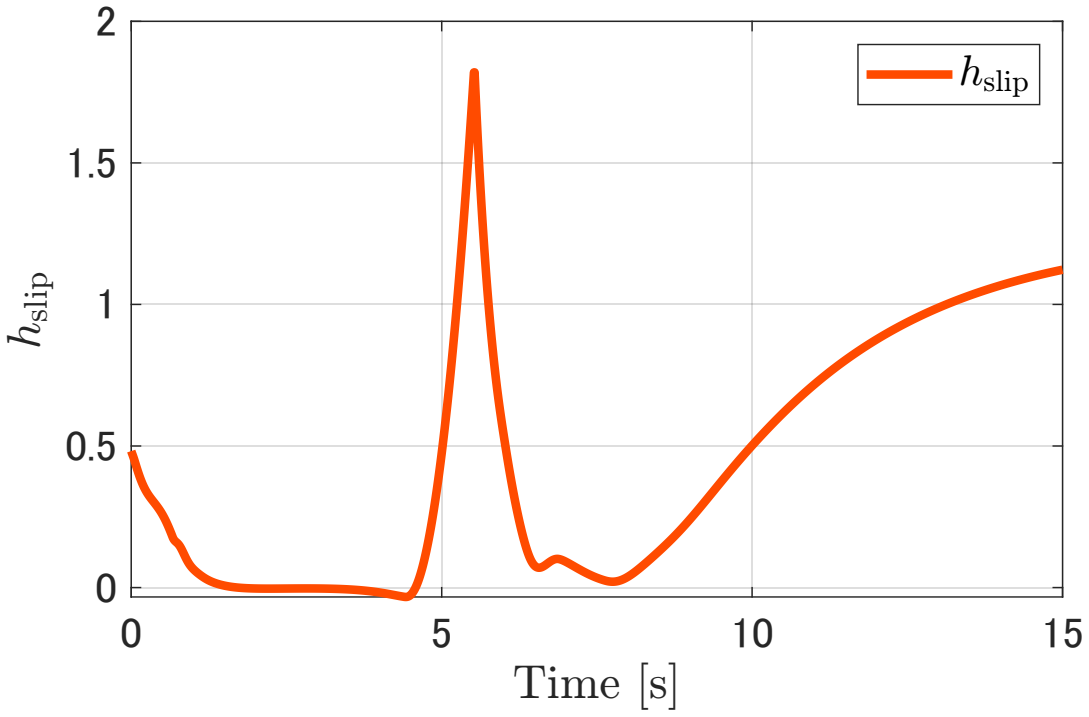

Figure 12. Sideslip CBF of the simulation result.